Characterization of the "guided light/photonic crystal" coupling by absorbance

Lucie Devys,, Géraldine Dantelle, Viacheslav Kubytskyi, H. Benisty, Thierry Gacoin

Characterization of the "guided light/photonic crystal" coupling by absorbance

Lucie Devys*[a], Géraldine Dantelle[a], Viacheslav Kubytskyi[a], Henri Benisty[b], Thierry Gacoin[a]

[a]Laboratoire de Physique de la Matière Condensée, UMR CNRS 7643 – Ecole Polytechnique – 91128 PALAISEAU Cedex, France

[b] Laboratoire Charles Fabry de l'Institut d'Optique, CNRS, Université Paris-Sud, Campus Polytechnique, RD 128, F-91127 Palaiseau Cedex, France

ABSTRACT

Considering luminescent TiO_2 films whose surface was imprinted with a 2D square shaped photonic crystal with different pattern depths (from 20 to 61 nm), we demonstrate the possibility to use simple absorption measurements to evaluate the efficiency of light extraction. Absorption spectra of the patterned systems show absorption peaks, evidencing the coupling between the photonic crystal structure and light guided within the film, in good agreement with 2D-RCWA simulations. The deeper the pattern depth, the stronger the coupling between the guided light and the photonic crystal. Using RCWA simulations, we show that it is possible to evaluate the extraction length, characteristic of the efficiency of light extraction, from the absorption spectra, in good agreement with direct measurements reported elsewhere.

Keywords: Extraction length, Paterning, Photonic crystal, RCWA simulation

1. INTRODUCTION

The addition of surface patterning on the top of a light-emitting device is largely studied to improve light extraction [1,2]. The efficiency of such a structure is determined by the coupling between the guided modes propagating in the device and the structure itself, which is characterized in the literature by the measurement of light extraction length, corresponding to the length of light propagation in the film before being extracted. The stronger the coupling, the shorter the extraction length.

Matioli et al.[3] demonstrates that the extraction length can be deduced from the width of the diffraction peaks observed on 2D emission maps in the case of GaN-based LEDs. However, such experiment requires a high-resolution angle-spectrum-resolved set-up. More recently a straightforward method to determine the extraction length was described by Devys and *al.*[4] based on the direct observation of the extinction of the guided mode. Nevertheless, all these characterizations require a dedicated optical bench which needs time to be set up and optimized.

Here, the idea is to show that we could benefit from an easy, though indirect, method to characterize the PhC efficiency on light extraction, based on light trasmission measurements, as light extraction and light injection are highly correlated. In essence, the process of light injection in a film is indeed the reverse of extraction as illustrated Figure 1. We show here that the efficiency of coupling between an incident beam and the pattern system can be easily determined by an absorption measurement in transmission configuration using a common laboratory UV-vis spectrometer apparatus. Light is not precisely absorbed by the film but diverted and "absorbance" lines appear on the absorption spectra. For this study, we consider a model system, consisting of a TiO_2 sol-gel layer doped with europium chelates deposited onto a glass substrate and an upper TiO_2 layer which is structured by nano-imprint lithography (NIL).

*lucie.devys@polytechnique.edu, phone +33 169 334 716

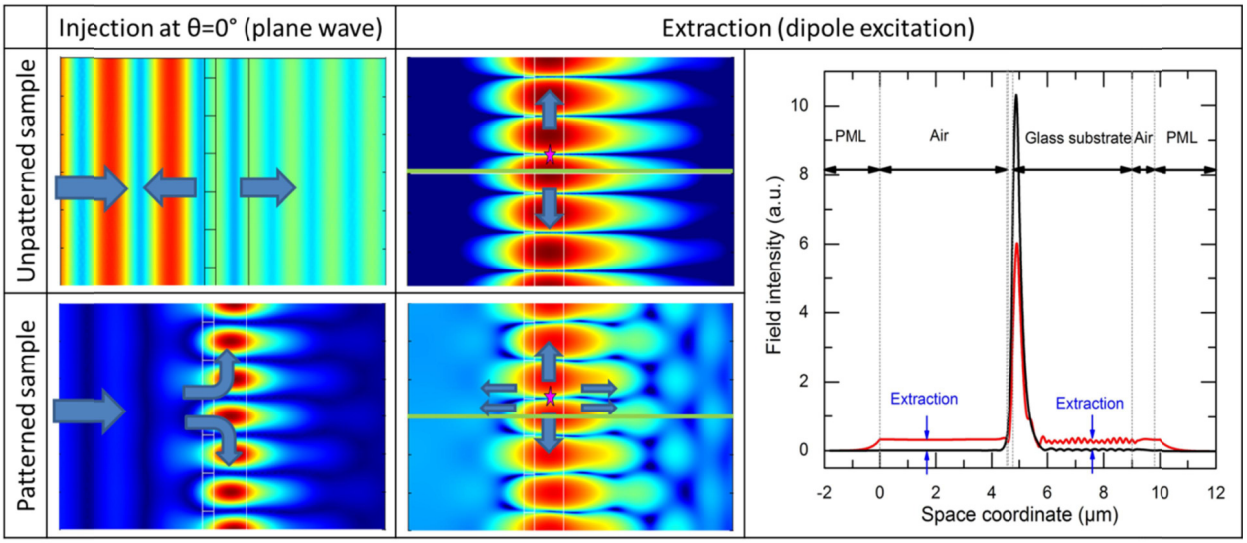

Figure 1: Similarity between the mechanisms of light injection and light extraction. The geometry of the system is explained on the graph. It consists of a TiO_2 layer of 236 nm on top a glass substrate. In the patterned case, the first 61 nm of the TiO_2 layer at the air interface is structured with a regular square geometry (period 400 nm). PML is a perfectly matched layer, which absorbs outgoing waves without reflection back to the computational domain.
Light injection: in the case of an unpatterned sample, whatever the wavelength of a normal incident wave, the light is either reflected or transmitted, there is no excitation of the guided mode in the TiO_2 layer. On the contrary, if the sample is structured, it exists a resonant wavelength which couples to the guide mode.
Light extraction: by introducing an emitting dipole (pink star) oriented perpendicularly to the layer (i.e. emission in the direction of the guided mode), a guided mode settles in the system. In the case of an unpatterned sample the light is completely trapped. Quite the reverse, if the sample is structured, the light at a given wavelength is extracted in the air and in the substrate. This resonant wavelength is the same as the one of the injection light experiment. The extraction of the light is shown in the plot of the intensity cuts along the green lines presented in the graph. The black curve corresponds to the cut of the non-structured sample, and the red one to the structured one. It shows that in the case of the structuration the intensity of the guided mode is attenuated because of the light escaped through the air and the substrate.

2. EXPERIMENTAL SECTION

2.1 Synthesis of TiO_2 thin film

Thin films of TiO_2 are produced according to the process described in [2].
Europium complexes $Eu(TTA)_3$ are synthesized following the process previously described by De Silva and al. [5]. This europium chelate is soluble in ethanol, thus it is simply dissolved in the TiO_2 sol with a concentration of 20 mg/mL. Excitation of such chelates occurs in the UV range and main emission is situated at 612 nm.
The sol containing the emitting molecules is deposited by spin-coating (2000 rpm, 30 s) onto glass substrates previously cleaned by an UV-Ozone treatment for 15 min at 50°C (Novascan cleaner). A thermal treatment (5 min at 110°C) allows the sol condensation. The obtained thin film of amorphous TiO_2 presents an optical index of 1.75, as measured by ellipsometry.

2.2 Surface patterning

On the top of the luminescent TiO_2 layer is deposited a second TiO_2 layer for surface structuration. This architecture is chosen in order to make sure that the same amount of emitters is present in the whole film despite the patterning. This second sol is different from the one used for the thin film containing the light emitters because the condensation of the latter appears too quickly. The solution of TiO_2 molecular precursors is complexed by acetylacetone which delays the condensation.[6] The obtained sol has a Ti concentration c_{max} of 1.2 10^{-3} mol/L. It is spin-coated (3000 rpm 30 s) onto the film doped with europium chelates. Before the TiO_2 condensation, a square polydimethylsiloxane (PDMS) mold with 400-nm period is applied onto the film surface. According to **Equation 1** and taking into consideration a 200-nm film

with a refractive index of 1.75 presenting a guided mode with an effective index n_{eff} of 1.58, such mold period a is perfectly appropriate to extract the main emission wavelength of the chelate (λ=620 nm) near the normal:

$$a = \lambda / n_{eff} \quad [1]$$

The system is then introduced into a NXR2500 imprinter from Nanonex, where it is heated at 110°C under a pressure of 20 PSI during 5 minutes. The grafting of trimethylchlorosilane (TMCS) on the mold prevents the adhesion between the PDMS and the TiO2 and facilitates the unmolding after cooling.
The thickness of the upper TiO_2 layer, d, is modified by changing the concentration of Ti precursors in the sol. Three different samples, Film A, B and C are prepared using respectively three different concentrations of Ti precursors, $c_{max}/4$, $c_{max}/2$ and c_{max} after dilution in isopropanol (Table 1).

2.3 Structural characterizations

Without going into details, the homogeneity and the quality of the films and the accuracy between the mold and the pattern imprinted in the TiO_2 was checked by atomic force microscopy (AFM) and scanning electron microscopy (MEB, Hitachi S4800 microscope). Moreover for each film the structural characteristics were precisely determined. The thickness of the layer containing the light emitters, e (Figure 2), was measured by profilometry (Dektak 150 profilometer) prior the deposition of TiO_2 sublayer. It is the same for all samples, with a value of 175 nm. This result was confirmed by ellipsometry (MM-16 Horiba Jobin Yvon) measurements. Moreover, AFM provides a precise measurement of the depth of the structure, d. The thicknesses e and $t+e$ of the layer(s) of TiO_2 are measured by scratching the surface after the deposit of one or two layers of TiO_2 and measuring the depth of the scratch by profilometry. For such measurements, an observation under optical microscope is required to make sure the film is cleanly removed and the underneath substrate is not scratched. The results are gathered in Table 1.

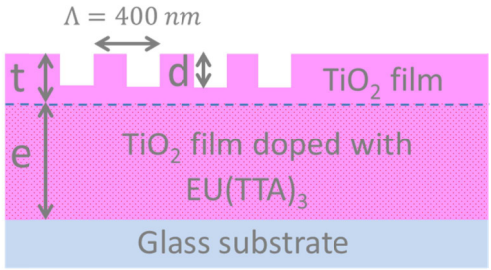

Figure 2 : Scheme of the structure under study.

	Sol concentration	**Film thickness *t+e* (nm, ±3)***	**Pattern depth *d* (nm, ±2)***	**t (nm) ****	**Effective index (TE mode)*****
Film A	$c_{max}/4$	200	22	25	1.569
Film B	$c_{max}/2$	209	38	34	1.577
Film C	c_{max}	253	61	78	1.598

Table 1: Structural characteristics of the three films. * corresponds to measured data; ** corresponds to deduced data; *** corresponds to calculated data[7]

2.4 Optical characterizations

The near-normal-incidence extinction is quantified using a Varian Cary 50 Scan UV-visible spectrometer. A measure is made on the patterned and on an unpatterned zone of each sample between λ=400 and 800 nm.

3. RESULTS

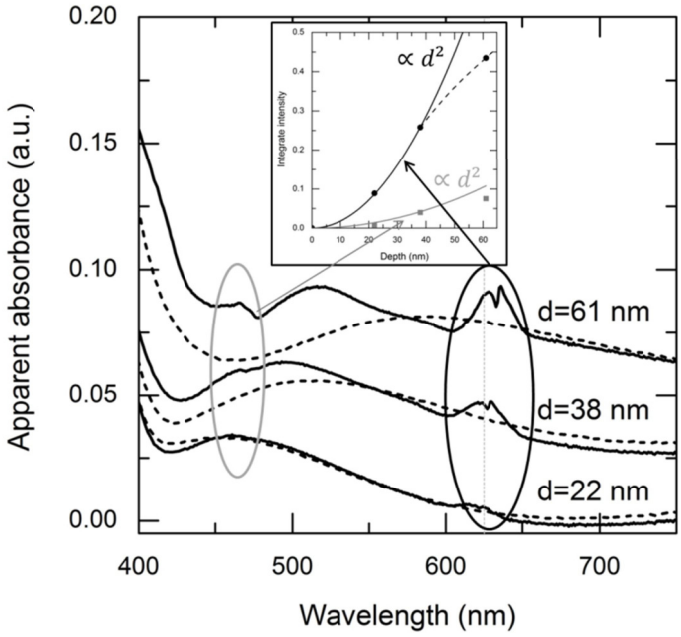

Figure 3: Apparent absorbance for the three films on a patterned (solid) and non-patterned zone (dashed). The spectra were artificially shifted for clarity reasons. Vertical line corresponds to λ=625 nm Inset: Area of the massifs at λ=625 nm (black) and at λ=450 nm (grey) as a function of the pattern depth.

The efficiency of the PhC is evaluated by studying the apparent absorbance spectra of the different films (Figure 3), in a patterned (solid line) and in a non-patterned (dashed line) area. For the patterned areas, the shape is similar for the three samples: a broad band between 400 nm and 550 nm and two peaks around 620 nm as predicted (Equation 1). It evidences that, at normal incidence, red light is coupled to the PhC and guided into the film through its two supported modes, TE and TM, associated for instance to the peaks at 621 nm and 630 nm for d=38 nm. We observe that the deeper the PhC, the stronger the coupling with the external beam. Film C, with d=61 nm, couples the impinging light with the highest efficiency. The integration of the peaks (Inset Figure 3) provides a more quantitative view of this evolution.

It is interesting to use the strength of the peak to check the predictions of the coupling factor known from Kazarinov theory[8]. The relevant overlap integral intervenes, in this theory (Equations A17-A19), through its square, and thus, the main trend for a given guided mode profile and a layer of variable height with modulated index is a d^2 dependence. By plotting the apparent absorbance area vs. pattern depth in inset Figure 3, we find good agreement with such a trend for the two first points –films A and B). Film C whose depth of 61 nm is a larger fraction of the wavelength ($\lambda/4n$~100 nm) lies below the extrapolation from films A and B.

Moreover by subtracting the absorbance measured on non-patterned zone (dashed lines on Figure 3) an unexpected weak broad band at λ=450 nm appears (Figure 4), which seems to follow the same evolution than one at λ=620 nm (see inset). However at this stage of the exploitation it is impossible to judge if this second massif has physical sense.

Furthermore a shift of the peak to the higher energies is observed when the effective index decreases: all features shift by $\Delta\lambda$~+10 nm from film A to film C, indicating a modification of the guided mode effective refractive index. The effective indices of the TE and TM guided modes $n_{eff}^{TE,TM}$ can be calculated using a 1D mode solver[7] for the different films considering that the average refractive index for the PhC is $1.6 = 1*f + 1.79*(1-f)$ with an air filling factor $f \sim 0.25$.[2] Results are reported on Table 1. The variations of the effective indices reflect the overall addition of matter that is made when adding the patterned layer. As we deal with deposited matter rather than etching, the deeper pattern in sample C corresponds to the larger amount of deposited matter on the luminescent layer, and thus the higher effective index. The shift observed is therefore consistent with [Equation 1], which predicts here a shift of the normal incidence extraction to the longer wavelengths for the higher refractive indices. It means that film C is the most efficient in terms of coupling with the incident light but it will mainly couple light at 630 nm for the near-normal incidence of interest.

In order to go further in the interpretation, 2D Rigorous Coupled Wave Analysis (RCWA) simulation was performed. [9] Firstly, the aim is to match the experimental curves obtained with the UV-vis spectrometer. In this perspective, we looked at the variations of the 0th-order transmission as a function of the wavelength, for a fixed incident angle, $\theta = 0°$. Figure 4 shows the result for a structure corresponding to Film C: 200 nm square holes ($n=n_{air}=1$) periodically (a=400 nm) distributed in a TiO_2 layer (n=1.75; d= 61 nm) on top of a continuous TiO_2 layer (n=1.75) and with a glass substrate (n=1.5). The thickness of each layer can be adjusted to match the experimental sample. The calculation is made for a TM and a TE incident wave, but considering the geometrical symmetries of the system the results are perfectly identical. The shape of the simulated curve is similar to the experimental one with the two characteristic peaks at 625 nm and 635 nm. The simulated curve also shows the two extra peaks at 450 nm, much less intense than the ones at 625 nm. This proves that the broad band at 450 nm previously described is not an artefact. Moreover, it will be seen later that those peaks disappear in the case of a 1D simulation. They are thus inherent to the existence of 2 dimensions in our system.

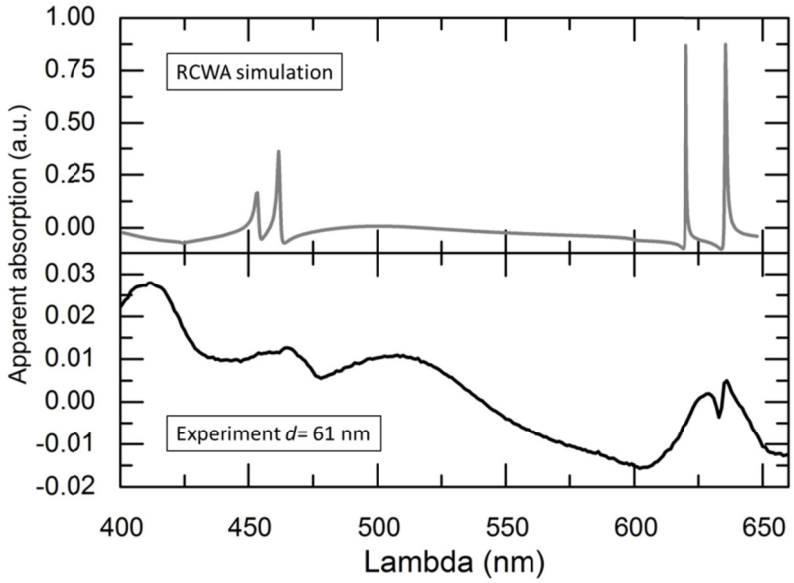

Figure 4: Apparent absorbance for Film C (d=61 nm) (black) and the corresponding 2D-RCWA simulations (grey) for an incident angle θ=0°. Note the peaks around 625 nm and 635 nm corresponds to coupling to the guided mode.

Furthermore, the width and the intensity of the simulated peaks are much thinner than the experimental one. This can be explained by some of the simplifications taken in the simulations, such as the zero NA (normal incidence) of the UV-vis spectrometer (NA<0.025 in the spectrometer used experimentally), its monochromaticity, the perfectly square shape of the patterning…

To investigate the role of the effects mentioned above, we first checked if by choosing a suitable system we could reasonably use 1D RCWA[10] simulation instead of 2D. For this new 1D system a square geometry was used, alternating n_{TiO2}=1.75 corresponding to a line full of TiO_2 and an effective index of n_{mean} = 1.375 corresponding to a line containing one half of TiO_2 and the other of air (Figure 4). As for the 2D, this geometry is deposited on top of a plain layer of TiO_2 and a glass substrate. The simulation is performed for a TE and a TM incident wave. The results are gathered in Figure 5. The adaptation of the system to the 1D involved the loss of symmetry, thus the results are different for a TE and a TM incident wave. Nevertheless, by combining the two polarizations of the 1D simulation, the two peaks around 625 nm and 635nm of the 2D simulation are perfectly reproduced. Even so the 1D calculation does not allow to reproduce the spectra around λ=450 nm. Thus the 1D-model is sufficient to study the effects occurring between 600 nm and 650 nm and in particular to investigate the impact of the dispersion in angle around the normal incidence on the features of the peaks. Moreover, there is a computational speed up of around 10 times for 1D to compare with 2D RCWA.

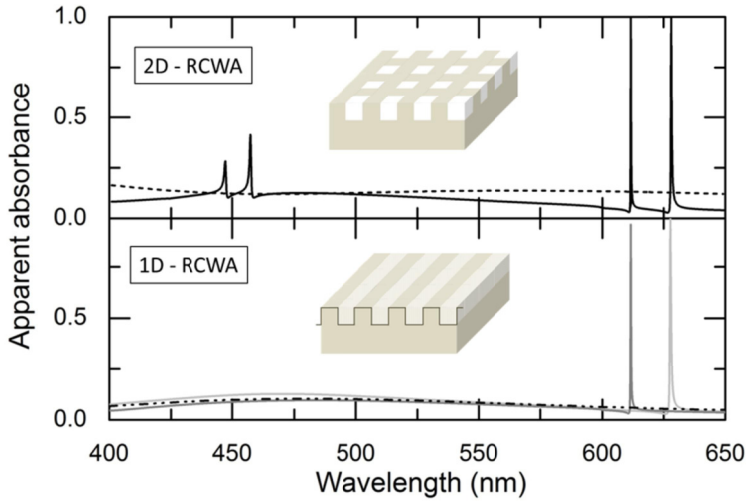

Figure 5: Comparison of the 1D and 2D RCWA simulations for a system corresponding to film B (*d*=38 nm). Top graph presents the 2D calculation for a pattern (solid black curve) and a non-patterned (dashed black curve) zone. Bottom graph presents the 1D calculation for a pattern zone and a TE (solid little grey curve) and a TM (solid dark grey curve) incident wave and a non-patterned (dashed black curve). The inserts show a schematic view of the system used for the 2D and 1D calculations.

With this aim, a system corresponding to the film B was simulated and the incident angle was scanned from θ=0° to 1.4 (thus by symmetry from -1.4° to 1.4°), corresponding to the larger angle permitted considering NA= 0.025, and with a step of 0.2°. The results are presented Figure 6. A split of each peak, increasing when we move away from the normal incidence is observed. In order to take into account the shape of the incident beam, the following weighting factor was used: $f_\theta = \sqrt{\theta^2{}_{max} - \theta^2}$. Thus, the angle aperture of the spectrometer explains the average and the enlargement of the experimental signal compared to the simulated one, but, as mentioned before, this may not be the only effect.

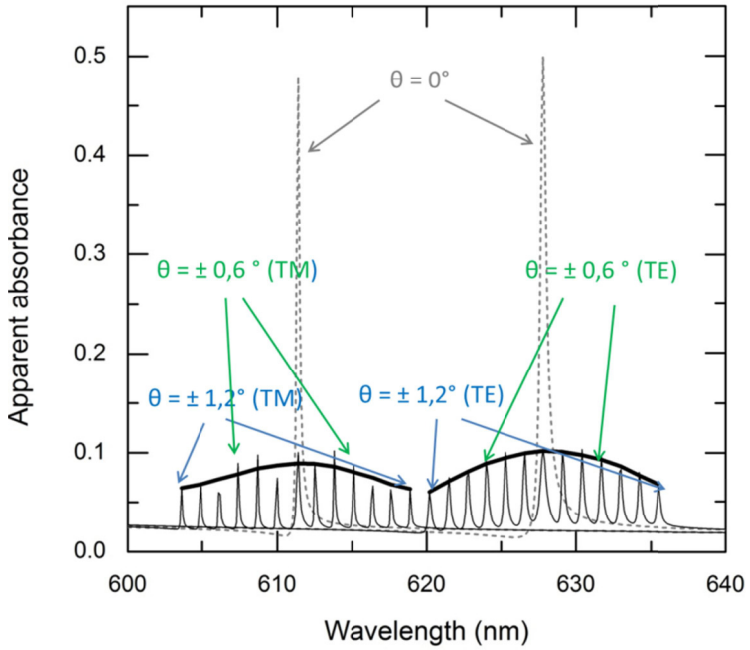

Figure 6: Explanation of broadening of experimental peaks seen in Figure 4 for λ=600:640 nm. Angle aperture spectrometer has beam divergence of around 1.4°.

Secondly, we attempted to exploit angular spectra for extraction length determination. Still considering the effective 1D system, the incident wavelength was fixed at λ=650 nm, and we scanned the 0th-order transmission as a function of the incident angle. The resonance wavelength previously determined was not considered to avoid side effects present at θ=0°. The simulated system is similar to the previous one, but the pattern depth *d* is modulated from 10 to 80 nm. For each depth, the full width at half maximum (FWHM, $\Delta\theta$) are determined and presented in Table 2. Moreover, Matioli's method, which relates the extraction length *Lext* to the width of the diffraction bands, can be applied in this case (Equation 2). [6]

$$L_{ext} = \frac{1}{k_0 \, \Delta\theta \, cos\theta} \qquad [2]$$

The extraction lengths (distance that light propagates in the film before being extracted) deduced from the simulations are presented on Figure 6. The order of magnitude of those values is consistent with the experimental one presented in the literature[4].
Moreover, as $\Delta\theta$ and the peak FWHM, $\Delta\lambda$, are related, the extraction length could theoretically be deduced from the experimental data as well. Yet, using a UV-visble spectrometer does not provide the required resolution. But since the evolutions of $\Delta\theta$ and of the peak area as a function of *d* are similar (Figure 2 and Table 2), the peak area (if we use the same spectrometer)is a sufficient measurement to compare quantitatively the coupling strength.

d *(nm)*	***FWHM Δθ (rad)***
10	2.56556E-5
20	1.99136E-4
40	7.57625E-4
60	0.00158
80	0.00246

Table 2: Measurements of the FWHM in radian for different depths, *d.*

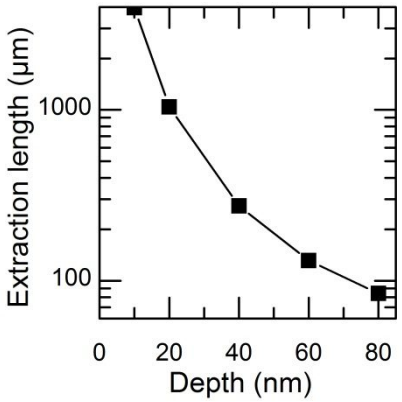

Figure 7 : Evolution of the extraction length as a function of pattern depth, calculated from the FWMH values of the simulated peaks by applying Equation 2.

4. CONCLUSION

We presented a simple experimental method to measure the efficiency of the PhC. Contrarily to the characterization describes in the literature, it does not need complex set up, a simple UV-vis spectrometer allows to get the essential data to feed a quest of an optimum PhC depth for light extraction.
Moreover we demonstrated both experimentally and numerically, the influence of the patterning on the light extraction for light emitting device. We found a good correspondence between experimental and numerical results.
The coupling increases proportionally to d^2 as predicted by Kazarinov for small modulation depths. It has been shown that extraction length is varying between hundred and few thousands of wavelengths of incident light for guided mode resonance. Our numerical approach can be used to furthersystem optimization and facilitating the experiment preparation.

[1] A. David, H. Benisty, C. Weisbuch, Rep Prog Phys **2012**, *75*, 126501.

[2] A. Revaux, G. Dantelle, D. Decanini, A.M. Haghiri-Gosnet, C. Weisbuch, T. Gacoin, J.P. Boilot, H. Benisty, Nanotechnology **2011**, *22*, 365701.

[3] E. Matioli, B. Fleury, E. Rangel, E. Hu, J. Speck, C. Weisbuch, J. Appl. Phys. **2010**, *107*, 053114.

[4] L Devys, G. Dantelle, A. Revaux, V. Kubytskyi, D. Paget, H. Benisty, T. Gacoin, submitted to Adv. Opt. Mat.

[5] C. de Silva, J. Maeyer, R. Wang, G. Nichol, Z. Zheng, Inorg. Chim. Acta 2007, 360, 3543.

[6] M. J. Hampton, S. S. Williams, Z. Zhou, J. Nunes, D.-H. Ko, J. L. Templeton, E. T. Samulski, J. M. Simone, Adv. Mater. 2008, 20, 2667.

[7] University of Twente, 1D-mode solver, http://wwwhome.math.utwente.nl/~hammer/oms.html

[8] R. Kazarinov, C. Henry, IEEE J. Quant. Electr. **1985**, *21*, 144.

[9] P. Kwiecien, 2D-RCWA, http://sourceforge.net/projects/rcwa-2d/

[10] P. Kwiecien, 1D-RCWA, http://sourceforge.net/projects/rcwa-1d/